

# A compact five-band patch antenna covering WLAN, WiMAX, X, and Ku-bands

Suthasinee Lamultree, Wutthipong Thanamalapong, Kanawat Nuangwongsa, Charinsak Saetiaw

Department of Electronics and Telecommunication Engineering, Faculty of Engineering, Rajamangala University of Technology Isan Khonkaen Campus, Khonkaen, Thailand

---

## Article Info

### Article history:

Received Feb 24, 2025

Revised May 12, 2025

Accepted May 26, 2025

---

### Keywords:

Bidirectional pattern antenna

Compact antenna

Five-band antenna

Multi-band antenna

Rectangular patch antenna

---

## ABSTRACT

This paper introduces a compact, low-profile, five-band antenna for wireless communication systems operating across 2.4/5 GHz WLAN, 3.5 GHz Wi-Max, and 7.5 GHz X- and Ku-band frequencies. The proposed antenna utilizes a novel configuration with a dual-overlapping rectangular patch coupled to a wide circular slot and an inverted L-shaped strip. Fabricated on a single-layer FR4 substrate ( $\epsilon_r=4.3$ , thickness=1.6 mm), the antenna employs a 50-ohm coplanar waveguide feed, resulting in a compact footprint of  $40 \times 40 \times 1.6$  mm<sup>3</sup>. Experimental measurements and simulations demonstrate a bidirectional radiation pattern covering five distinct frequency bands: 2.4-2.485 GHz, 3.4-3.6 GHz, 5.15-5.825 GHz, 7.25-8.4 GHz, and 13.4-17.7 GHz. The antenna exhibits a return loss better than 10 dB across all bands and provides average gains of 1.78 dBi, 3.04 dBi, 3.4 dBi, 4.27 dBi, and 4.46 dBi, respectively. These results confirm the successful development of a five-band antenna with excellent performance characteristics, making it a promising candidate for 2.4/5 GHz WLAN, Wi-Max, and X- and Ku-band satellite communications, with automotive vehicles being one example.

*This is an open access article under the [CC BY-SA](https://creativecommons.org/licenses/by-sa/4.0/) license.*



---

## Corresponding Author:

Suthasinee Lamultree

Department of Electronics and Telecommunication Engineering, Faculty of Engineering

Rajamangala University of Technology Isan Khonkaen Campus

Khonkaen, 40000, Thailand

Email: suthasinee.la@rmuti.ac.th

---

## 1. INTRODUCTION

The rapid expansion of wireless communication applications drives the increasing demand for compact, multi-functional, multi-band antennas. These advanced antennas are crucial for modern wireless systems [1]-[4], supporting diverse technologies such as 2.4/5 GHz WLAN, WiMAX, IoT, LTE, sub-6 5G, 6G, and X/Ku-band satellite communications. Their compact and versatile design is essential for the growing range of wireless applications. Effective antenna design is critical for multi-band performance, influencing gain, bandwidth, and efficiency. Modern wireless systems depend on these antennas' ability to operate across diverse frequency ranges, achieved through innovative materials and geometries [5]-[9]. However, optimizing these antennas for specific applications while ensuring consistent performance across all intended bands remains a significant challenge.

Several techniques for achieving multi-band operation include metamaterials utilizing FR4 substrate and complementary split ring resonators [2]; fork-shaped radiating components [4]; electromagnetic-transparent cascade comb dipole antennas for shared-aperture base station arrays [10]; partial ground planes with dual-sided reverse stage stairs [11]; and artificial magnetic conductor techniques [12]. Other approaches include side-by-side placement multi-radiators [13] and embedded schemes [14], meander lines and slots

[14], [15], using different antenna types for different bands [16], multi-radiating components [17], stub tuning [5], [18], and slots with loading stubs [19]. Further enhancements can be achieved by modifying ground planes [20], [21], using slotted geometries [20], [22], adjusting feeding lines with parasitic elements [23], employing the asymmetric coplanar strip-fed technique [24], exploring various modes with slot tuning [25], and using a fractal technique [3], [26]. These strategies contribute to improving the functionality and efficiency of multi-band antennas.

Bidirectional antennas are crucial for wireless communication in specific environments like streets, highways, skywalks, corridors, tunnels, and subway stations [14], [18], [27], ensuring adequate coverage. Several techniques achieve bidirectional propagation. These include utilizing wide slots to manipulate omnidirectional radiation [18], the spoof surface plasmon polariton (SPP) method for wideband end-fire antennas [28], reshaping slot antenna radiation patterns using characteristic mode analysis [29], and combining two unidirectional antennas, such as back-to-back frequency scanning tapered slot antenna (FSTSA) elements [30]. The multi-resonance principle, combining multiple bow-tie antennas, is another approach [31]. These methods improve communication efficiency in environments requiring robust signal coverage.

This paper presents a bidirectional antenna design integrating a dual-overlapping rectangular patch (DORP) within a wide circular slot (WCS) and an inverted-L shape strip (ILSS), fed by a coplanar waveguide (CPW). This compact antenna operates across five bands, supporting 2.4-2.484 GHz for 2.4 GHz WLAN, 3.4-3.6 GHz for WiMAX, 5.15-5.825 GHz for 5 GHz WLAN, 7.25-8.4 GHz for X-band, and 13.4-17.7 GHz for Ku-band applications (satellite communications and radar). Its multi-band capability makes it suitable for urban outdoor mobility, receiving signals from WLAN/WiMAX towers and satellites. It can also be used in high-gain antenna arrays for satellite communications. Initial theoretical design parameters were calculated (section 2) and then simulated in CST microwave studio [32]. The final design parameters were determined through an iterative simulation process.

## 2. THE PROPOSED METHOD

### 2.1. Antenna layout and formulas

This section details the design of a five-band bidirectional patch antenna (FBBPA), an extension of our previously developed tri-band design (TBBPA) [18] for 2.4/5 GHz WLAN and Ku-band operation. The TBBPA (Figure 1(a) [18]) consisted of a rectangular radiating patch (RRP) of width  $w_r$  and length  $l_r$  within a WCS of radius  $r$ . This WCS was employed to achieve bidirectional radiation patterns. An ILSS with dimensions  $l_1$ ,  $l_2$ , and  $l_3$ , positioned at a height  $p$  above the ground plane, was used to tune impedance matching at the lower frequency band. For the transition to a five-band operation, as depicted in Figure 1(b), a smaller RRP (with dimensions  $w_{r1}$  and  $l_{r1}$ ) was strategically placed above the original RRP. Its precise positioning, including spacing ( $s_r$ ) and center point ( $p_r$ ), was meticulously designed to introduce additional resonances. Both antennas were fabricated on a cost-effective FR4 substrate (width  $w$ , length  $l$ , thickness  $h=1.6$  mm, relative permittivity 4.3) and fed by a 50- $\Omega$  CPW with a feed line length of  $l_f$ , width of  $w_f$ , gap of  $g$ , and ground plane length  $l_g$  beneath the RRP. The TBBPA achieved a 10 dB return loss across 2-2.56 GHz, 4.42–6.82 GHz, and 13.26-17.70 GHz, with an additional resonance of around 8.9 GHz (Figure 2, dashed line). To expand this to five-band operation and introduce two new resonances at approximately 3.5 GHz and 8 GHz (represented by the solid line in Figure 2), the smaller RRP was added as described. The following section analyzes the impact of the upper RRP parameters ( $l_{r1}$ ,  $w_{r1}$ ,  $s_r$ , and  $p_r$ ).

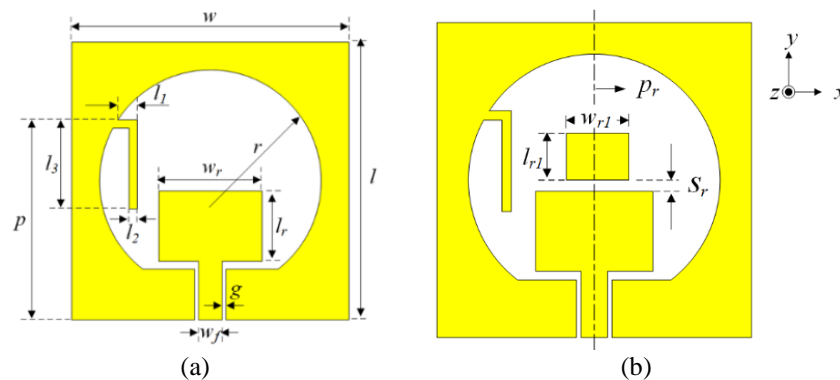


Figure 1. Development of the designed antenna: (a) TBBPA [18] and (b) FBBPA

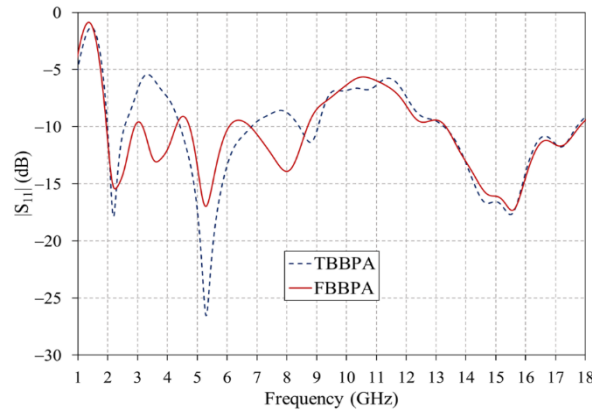


Figure 2. Simulated  $|S_{11}|$  of the TBBPA and FBBPA

Initial antenna dimensions were calculated using established formulas [18], [33]. The lower rectangular patch width ( $w_r$ ) was calculated for a 5.5 GHz resonance:

$$w_r = \frac{c}{2f_r} \sqrt{\frac{2}{\epsilon_r + 1}} \quad (1)$$

where  $w_r$  was the rectangular patch width,  $c$  was the speed of light,  $f$  was a resonant frequency (5.5 GHz), and  $\epsilon_r$  was the relative permittivity of the FR4 substrate (a value of 4.3). The lower rectangular patch length ( $l_r$ ) was then calculated:

$$l_r = \frac{c}{2f_r \sqrt{\epsilon_{reff}}} - 0.824h \left[ \frac{(\epsilon_{reff} + 0.3)(w_r + 0.264h)}{(\epsilon_{reff} - 0.258)(w_r + 0.8h)} \right] \quad (2)$$

where  $l_r$  was the patch length;  $\epsilon_{reff}$  was the effective dielectric constant of the substrate, and  $h$  was the substrate thickness.

$$\epsilon_{reff} = \frac{\epsilon_r + 1}{2} + \frac{\epsilon_r - 1}{2} \sqrt{1 + \frac{12h}{w_r}} \quad (3)$$

These calculations, which account for fringing effects, yielded initial dimensions of  $w_r=17$  mm and  $l_r=12$  mm. The upper rectangular patch dimensions ( $w_{r1}$  and  $l_{r1}$ ) for a 7.5 GHz resonance were calculated similarly, resulting in  $w_{r1}=12$  mm and  $l_{r1}=8$  mm. In addition, the feed line width ( $w_f$ ) and length ( $l_f$ ) for 50- $\Omega$  impedance matching were calculated using (4) and (5) from [18], [33].

$$w_f = \frac{2h}{\pi} \left\{ \left( \frac{60\pi^2}{Z_0 \sqrt{\epsilon_r}} \right) - 1 - \ln \left( \frac{120\pi^2}{Z_0 \sqrt{\epsilon_r}} - 1 \right) + \frac{\epsilon_r - 1}{2\epsilon_r} \left( \ln \left( \frac{60\pi^2}{Z_0 \sqrt{\epsilon_r}} - 1 \right) + 0.39 - \frac{0.61}{\epsilon_r} \right) \right\} \quad (4)$$

where  $B = 60\pi^2 (Z_0 \sqrt{\epsilon_r})^{-1}$ ,  $Z_0$  is the characteristic impedance of 50  $\Omega$ .

$$l_f = \frac{\lambda}{4\sqrt{\epsilon_{eff}}} \quad (5)$$

A feed line width  $w_f$  of 3 mm and length  $l_f$  of 8 mm were chosen. A 0.4 mm gap ( $g$ ) between the feed line and ground plane was selected to achieve a 50- $\Omega$  impedance, based on (6)-(10) from [34].

$$Z_0 = \frac{30\pi K'(k)}{\sqrt{\epsilon_{eff}} K(k)} \quad (6)$$

where  $K(k)$  and  $K'(k)$  are the complete elliptic integral of the first kind,

$$K(k) = \int_0^{\phi} \frac{d\theta}{\sqrt{1-k^2 \sin^2 \theta}} \begin{cases} 0 \leq k^2 < 1 \\ 0 \leq \phi < \frac{\pi}{2} \end{cases} \quad (7)$$

$$K'(k) = K(k') = \sqrt{1-k^2} \quad (8)$$

where the ratio of  $K(k)/K'(k)$  and  $k$  is defined as:

$$\frac{K(k)}{K'(k)} = \begin{cases} \frac{\pi}{\ln[2(1+\sqrt{k})/(1-\sqrt{k})]} & 0 \leq k \leq 0.707 \\ \frac{1}{\pi} \ln[2(1+\sqrt{k})/(1-\sqrt{k})] & 0.707 \leq k \leq 1 \end{cases} \quad (9)$$

and

$$k = \frac{w_f}{(2g+w_f)} \quad (10)$$

The substrate dimensions were set to  $40 \times 40 \text{ mm}^2$  ( $w \times l$ ) for a compact design. The WCS radius ( $r$ ) was designed for the dominant  $\text{TE}_{11}$  mode at 2.45 GHz using (11) [18], [33]:

$$r = \frac{18,412}{f_r 2\pi \sqrt{\mu_0 \epsilon_0}} \quad (11)$$

where  $\mu_0$  was the permeability in free space, and  $\epsilon_0$  was the permittivity in free space.

A radius of 17 mm was used. The ground plane length ( $l_g$ ) beneath the radiating patch was set to 7 mm. A single-arm ILSS with width  $l_1$ , thickness  $l_2$ , and length  $l_3$  was attached to the inner wall of the WCS at position  $p$  (Figure 1(a)) to generate resonance at 2.45 GHz. The total ILSS length ( $l_1 + l_3$ ) was approximately one-quarter of the wavelength at 2.45 GHz [18].

## 2.2. Key parameter effects

This section describes the design rationale and structure of the developed antenna, focusing on the addition of the upper RRP. The proposed antenna (Figure 1(b)) builds upon a TBBPA, which comprises a lower RRP within a WCS integrated with an ILSS and fed by a 50-Ohm CPW. The TBBPA resonates at 2.2 GHz (-17.85 dB), 5.31 GHz (-26.51 dB), and 15.49 GHz (-17.69 dB). A smaller RRP was added above the existing one to introduce additional resonances. Initial parameters for this upper RRP were  $w_{r1}=12 \text{ mm}$ ,  $l_{r1}=8 \text{ mm}$ , and  $s_r$  and  $p_r=0 \text{ mm}$ . This addition generates two new resonant frequencies. Subsequent adjustments to the upper RRP parameters ( $l_{r1}$ ,  $w_{r1}$ ,  $s_r$ , and  $p_r$ ) were performed to optimize their performance within the final FBBPA design.

The effect of  $w_{r1}$  on the reflection coefficient ( $|S_{11}|$ ) was initially assessed by varying its length (10, 12, and 14 mm) while holding all other parameters constant, as shown in Figure 3. Changes in  $w_{r1}$  significantly influenced the fourth frequency band (7.5 GHz). Decreasing  $w_{r1}$  causes a downward shift in the lower resonant frequency, potentially merging the third and fourth bands. Therefore,  $w_{r1}=12 \text{ mm}$  was selected for further analysis of the remaining parameters.

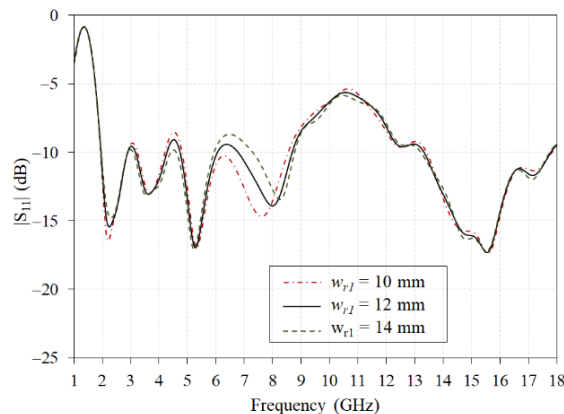


Figure 3. The effect of  $w_{r1}$  on  $|S_{11}|$

After analyzing the effect of  $w_{rl}$ , the impact of  $l_{rl}$  on  $|S_{11}|$  was investigated by varying its length to 6, 8, and 10 mm as depicted in Figure 4. The results show that  $l_{rl}$  primarily affects the second, third, and fourth frequency bands. Decreasing  $l_{rl}$  lowers the resonant frequency, deepening the  $|S_{11}|$  and potentially merging the third and fourth bands below 6 GHz. Conversely, at higher frequencies, a shorter  $l_{rl}$  shifts the higher resonant frequency upwards. While  $l_{rl}=6$  mm and  $l_{rl}=10$  mm achieve a 10 dB return loss across four bands,  $l_{rl}=6$  mm merges the second and third bands, and  $l_{rl}=10$  mm merges the third and fourth. Therefore,  $l_{rl}=8$  mm was chosen as the optimal value for subsequent analysis. The next step involves investigating the positioning of the upper RRP.

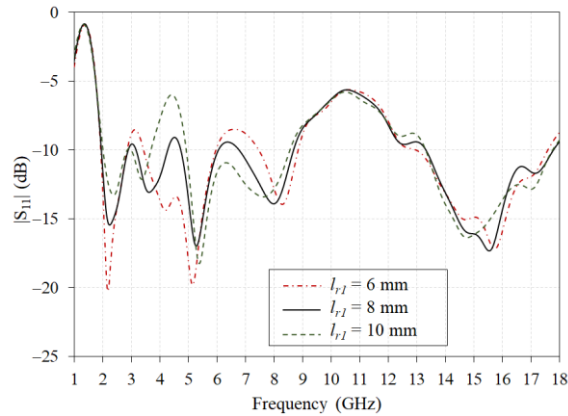


Figure 4. The effect of  $l_{rl}$  on  $|S_{11}|$

Figure 5 illustrates the impact of the spacing ( $s_r$ ) between the lower RRP and the upper RRP as the upper RRP is moved upward by distances of 0, 1, and 2 mm. The results indicate that increasing the space improves  $|S_{11}|$  for the third band; however, it negatively affects  $|S_{11}|$  for the second band and causes an upward shift in the higher resonance frequency for the fourth band. As a result, a spacing ( $s_r$ ) of 0 mm is chosen as the optimal configuration.

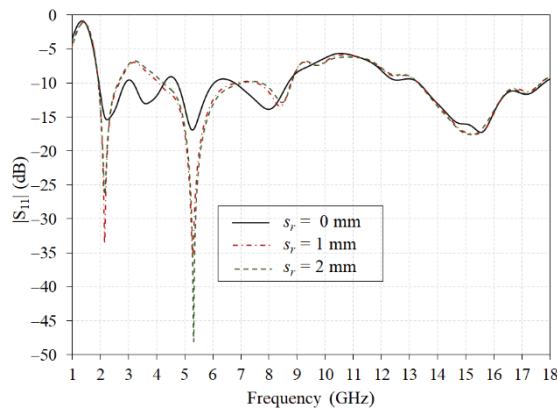
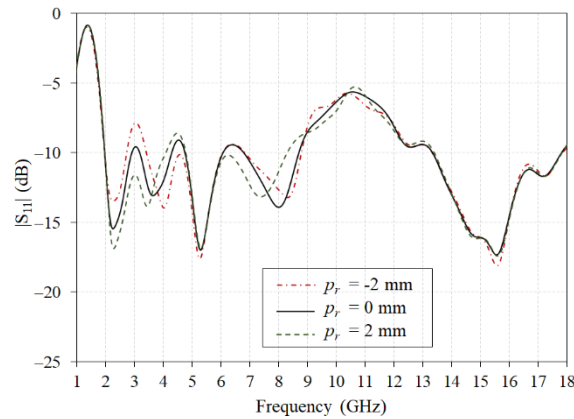


Figure 5. The effect of  $s_r$  on  $|S_{11}|$

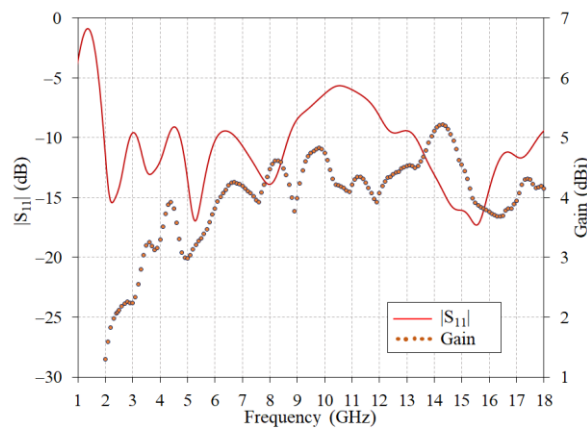
Next, the effect of shifting the upper RRP horizontally to the left (-) and right (+) on  $|S_{11}|$  is examined, as depicted in Figure 6. The parameter  $p_r$  is adjusted to -2, 0, and 2-mm values. The findings reveal that moving the upper RRP horizontally affects the first, second, and fourth bands, while the third and fifth bands remain unchanged. Specifically, shifting to the left at -2 mm results in a deterioration of  $|S_{11}|$ , particularly at frequencies below 3 GHz, and causes the resonance frequency to shift upward. In contrast, moving to the right produces different effects. Notably,  $p_r$  of -2 mm tends to merge the second and third bands, whereas  $p_r$  of 2 mm merges the first and second bands. Therefore, the optimal design positions the upper RRP at the center of the lower RRP ( $p_r = 0$ ).

Figure 6. The effect of  $p_r$  on  $|S_{11}|$ 

The optimized FBBPA parameters, derived through CST simulations, are summarized in Table 1. As shown in Figure 7, the antenna achieves a 10 dB return loss across five bands: 1.9-2.8 GHz, 3.1-4.2 GHz, 4.7-6.0 GHz, 6.7-8.6 GHz, and 13.3-17.7 GHz. The antenna exhibits a bidirectional radiation pattern. The simulated gain ranges from 1.3 to 2.26 dBi, 2.34 to 3.73 dBi, 2.98 to 3.82 dBi, 3.92 to 4.62 dBi, and 3.69 to 5.22 dBi for each respective band. The corresponding radiation efficiencies range from 61% to 78%, 75% to 86%, 82% to 86%, 78% to 80%, and 68% to 77%.

Table 1. Final FBBPA parameter values

Variable	Parameter	Physical Size (mm)
$w$	The width of the substrate	40
$l$	The length of the substrate	40
$r$	The radius of the wide circular slot	17
$l_r$	The rectangular length of the lower RRP	10
$w_r$	The rectangular width of the lower RRP	19
$l_{r1}$	The rectangular length of the upper RRP	8
$w_{r1}$	The rectangular width of the upper RRP	12
$s_r$	The spacing between the upper and lower RRPs	0
$l_1$	The short length of ILSS	2
$l_2$	The width of ILSS	1
$l_3$	The length of ILSS	13
$p$	The position height of ILSS	30
$h$	The thickness of the substrate	1.6
$l_f$	The length of the feeding strip	8
$w_f$	The width of the feeding strip	3
$l_g$	The length of the ground plane	7
$g$	The gap between the feed line and the ground plane	0.4

Figure 7. Simulated  $|S_{11}|$  and gain of the FBBPA

### 3. RESULTS AND DISCUSSION

To validate the simulation results, an FBBPA prototype was fabricated according to the dimensions specified in Table 1 (Figure 8). Figure 8(a) shows the schematic model, and Figure 8(b) shows the fabricated prototype. The FBBPA prototype was soldered to a 50-ohm subminiature version A connector for connection to a coaxial feed line. An E5063A network analyzer was used to measure the reflection coefficient ( $|S_{11}|$ ), radiation patterns, and antenna gain.

Figure 9 illustrates the numerical and experimental values of  $|S_{11}|$ . Both values exhibit a similar trend, with most numerical values aligning closely with the experimental results. The observed deviation can likely be attributed to a slight difference in the setups: the experimental configuration included a 50-ohm subminiature version A connector, which was not reflected in the simulation. This approach was intentional, as the focus was on examining the intrinsic properties of the antenna itself, minimizing the influence of external components, and reducing simulation time. The simulated  $|S_{11}|$  results remained below -10 dB across the frequency ranges of 1.9-2.8 GHz, 3.1-4.2 GHz, 4.7-6.0 GHz, 6.7-8.8 GHz, and 13.3-17.7 GHz. In comparison, the measured  $|S_{11}|$  results were below -10 dB across the ranges of 1.9-2.7 GHz, 3.3-3.8 GHz, 4.7-5.8 GHz, 7.2-8.4 GHz, and 12.2-18 GHz.

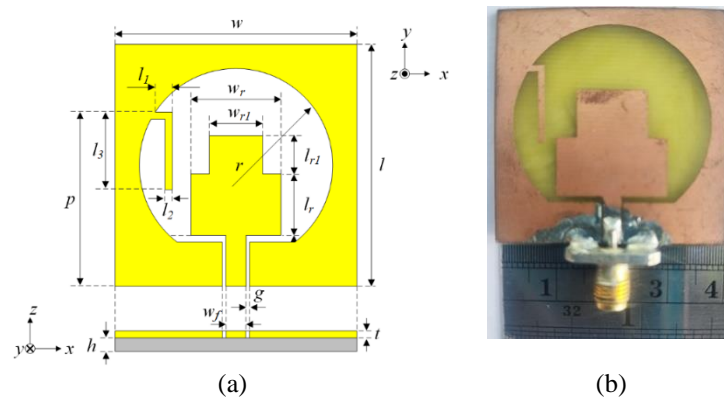


Figure 8. The FBBPA: (a) layout model and (b) prototype

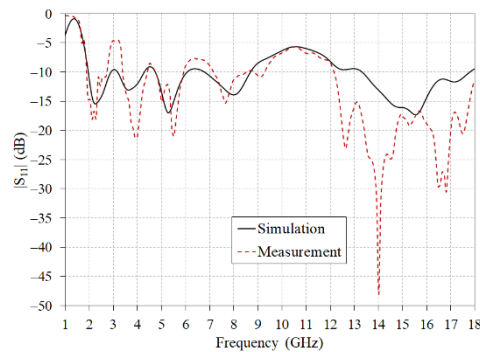


Figure 9. Comparing simulated and measured  $|S_{11}|$

Beyond impedance characteristics, the 3D and normalized radiation patterns of the proposed FBBPA in the  $xz$ - and  $yz$ -planes were measured at 2.45, 3.5, 5.5, 7.5, and 16.7 GHz as plotted in Figures 10(a) to (e), respectively. The FBBPA exhibited a bidirectional radiation pattern with distinct main beam shapes for each band. At 2.45 GHz and 3.5 GHz, the main beam propagated in both forward and backward directions as depicted in Figures 10(a) and 10 (b). However, at 5.5 GHz, 7.5 GHz, and 16.7 GHz, the main beam was elevated by approximately  $35^\circ$  as exhibited in Figures 10(c) to (e). Linear polarization with cross-polarization levels below -30 dB was observed across all bands. Simulated and measured gains were, respectively: 2.1/1.79 dBi at 2.45 GHz; 3.24/3.36 dBi at 3.5 GHz; 3.36/3.36 dBi at 5.5 GHz; 4.02/3.44 dBi at 7.5 GHz; 4.86/5.51 dBi at 13.7 GHz; and 3.85/3.46 dBi at 16.7 GHz. Simulated radiation efficiencies were at least 61%, 75%, 82%, 78%, and 68% for the five bands, respectively. Note that the radiation pattern in the fifth band is measured at the upper edge of the frequency band.

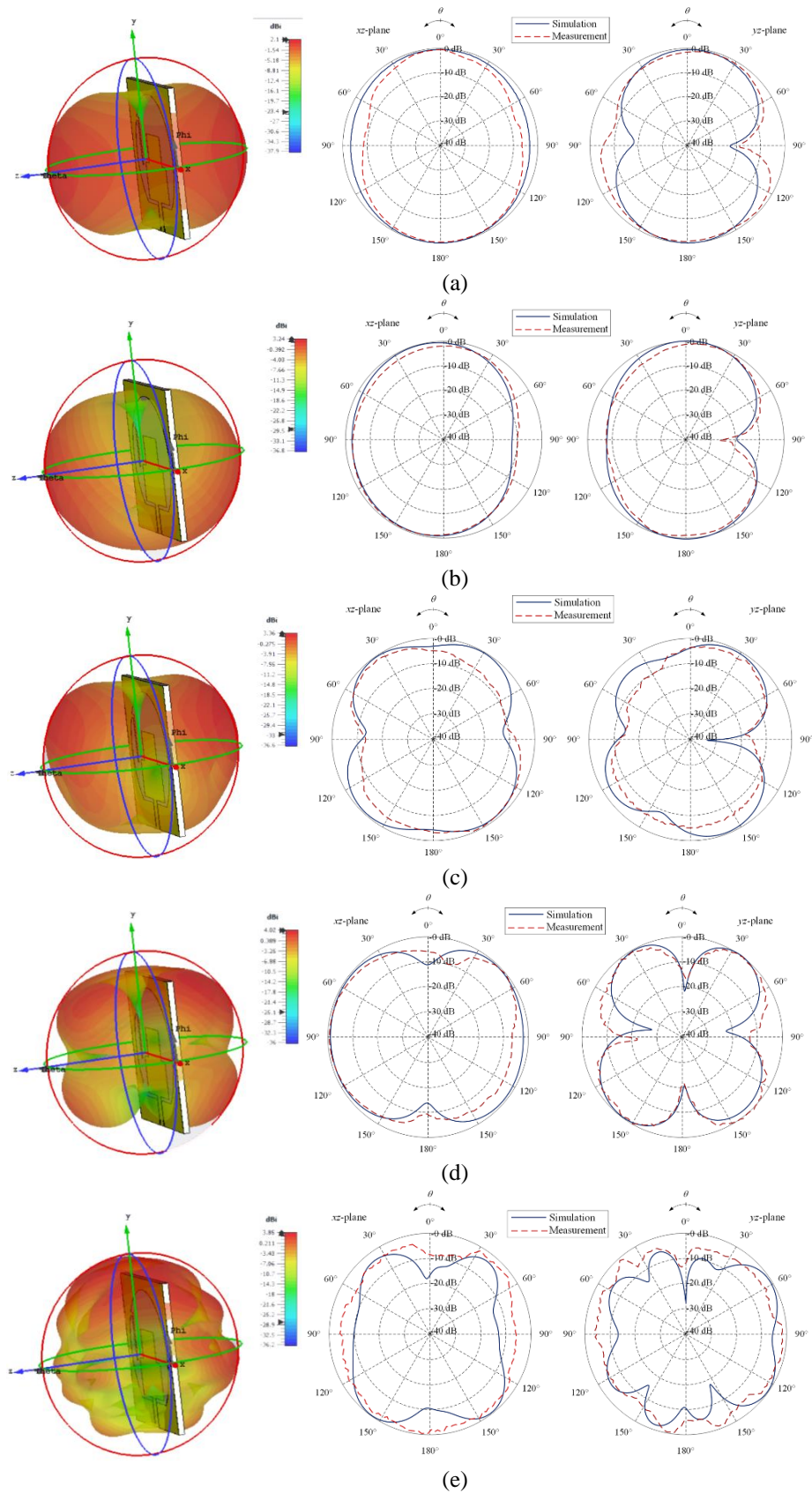


Figure 10. Simulated and measured radiation patterns at: (a) 2.45 GHz, (b) 3.5 GHz, (c) 5.5 GHz, (d) 7.5 GHz, and (e) 16.7 GHz



The electrical performance of the proposed multi-band antenna was compared to existing omnidirectional, unidirectional, and bidirectional antennas, as summarized in Table 2. The proposed design demonstrates a more compact form factor and simplified structure relative to the five-band antenna described in [3] (omnidirectional, FR4 substrate), with comparable gain performance across the considered frequency bands. Compared to the tri-band antenna arrays in [13] and [16] (both constructed using RO4003), the proposed design offers a more compact size. While the antenna in [13] (bidirectional) exhibits higher gain, it demonstrates lower gain in its lower frequency band. The antenna in [16] (unidirectional) is more complex in structure. Compared to the antenna in [18] (FR-4 substrate, bidirectional), the proposed FBBPA achieves a smaller relative size, supports more resonant bands, and exhibits slightly better gain across all operational bands, despite operating at the highest frequency. Compared to the antenna in [23] (omnidirectional, thinnest substrate), the proposed design shows slightly lower gain across all the same frequency bands. The antenna in [31] (flexible materials, complex structure) provides a stable bidirectional pattern with higher gain but is limited to a single frequency band. Overall, the proposed antenna distinguishes itself by its compact relative electrical size, the maximum number of resonant bands supported, and its notable gain performance across all operational bands.

Table 2. Performance comparison with existing designs

References	Size (mλ)	Substrate of material	Pattern	-10 dB bandwidth.	Gain (dBi)	Complexity
[3]	45×45×0.97	FR4	Nearly omnidirectional	1.81–1.85 GHz, 2.76–2.82 GHz, 2.90–2.98 GHz, 4.24–4.44 GHz, 5.75–6 GHz	1.38/ 2.67/ 6.01/ 3.71/ 3.72	medium
[13]	31×28×1.21	RO4003	Bidirectional	840–924 MHz, 3–3.74 GHz, 4.9–5.54 GHz,	1/ 6/ 10	low
[16]	208×71×12	RO4003	Unidirectional	1.85–2.15 GHz, 3.4–3.6 GHz, 5.4–5.6 GHz	6.5/ 5.5/ 5	high
[18]	28×28×1.12	FR-4	Bidirectional	2.1–2.7 GHz, 4.82–6.1 GHz, 12.73–18 GHz	2.35/ 4.41/ 4.71	low
[23]	30×13×0.03	Rogers5880	Omnidirectional	0.64–0.71 GHz, 1.38–1.43 GHz, 2.26–2.44 GHz, 3.60–3.72 GHz, 5.36–5.71 GHz	-1/ 0.99/ 2.27/ 3.46/ 4.81	low
[31]	35×33×0.02	PET film	Bidirectional	1.23–2.88 GHz,	3.8	medium
This work	25×25×1.01	FR-4	Bidirectional	1.9–2.7 GHz, 3.3–3.8 GHz, 4.7–5.8 GHz, 7.2–8.4 GHz, 12.2–18 GHz	1.79/ 3.36/ 3.44/ 5.51/ 3.46	low

λ means a free-space wavelength at the lowest operated frequency.

In this study, a single antenna was examined, designed, analyzed, and implemented, and its impact on fundamental antenna theory was illustrated through laboratory testing. The evaluation included the antenna's 10 dB return loss, radiation pattern, and gain. Furthermore, this work presents important insights into antenna design and its applications. Future improvements to the FBBPA, including optimized high-frequency material selection and MIMO/array configurations, are recommended for enhanced performance.

#### 4. CONCLUSION

This study presents the design and implementation of a compact, bidirectional pattern, five-band antenna covering 2.4/5 GHz WLAN, 3.5 GHz WiMAX, 7.5 GHz X-band, and 13.4-17.7 GHz Ku-band applications. The antenna features dual-overlapping rectangular patches, a wide circular slot, and an inverted L-shaped strip, and is fed by a 50-ohm coplanar waveguide. A bidirectional radiation pattern and a return loss below -10 dB are achieved across all five bands. The good agreement between simulated and measured results validates the design. Measured gains are 1.79 dBi (2.45 GHz), 3.36 dBi (3.5 GHz), 3.36 dBi (5.5 GHz), 3.44 dBi (7.5 GHz), 5.51 dBi (13.7 GHz), and 3.46 dBi (16.7 GHz), closely correlating with simulated gains of 2.1 dBi, 3.24 dBi, 3.36 dBi, 4.02 dBi, 4.86 and 3.85 dBi, respectively. This proposed antenna demonstrates promising performance for multi-band wireless communication systems. This research

advances multifunctional wireless communication by providing an efficient five-band bidirectional pattern antenna solution, supporting current demands in WLAN, WiMAX, and satellite communication systems. Moreover, this development lays a foundation for the future integration of mobile internet, IoT connectivity, radar, and satellite technologies.

### ACKNOWLEDGEMENTS

We extend our sincere gratitude to Asst. Prof. Dr. Adirek Jantakun for his expert guidance on graphical elements.

### FUNDING INFORMATION

This research project is supported by Science Research and Innovation Fund Agreement No. FF68/KKC/024.

### AUTHOR CONTRIBUTIONS STATEMENT

This journal uses the Contributor Roles Taxonomy (CRediT) to recognize individual author contributions, reduce authorship disputes, and facilitate collaboration.

Name of Author	C	M	So	Va	Fo	I	R	D	O	E	Vi	Su	P	Fu
Suthasinee Lamultree	✓	✓		✓	✓	✓	✓	✓	✓	✓	✓	✓		✓
Wutthipong Thanamalapong			✓			✓	✓	✓	✓					
Kanawat Nuangwongsa					✓					✓			✓	
Charinsak Saetiaw		✓	✓							✓				✓

C : Conceptualization

M : Methodology

So : Software

Va : Validation

Fo : Formal analysis

I : Investigation

R : Resources

D : Data Curation

O : Writing - Original Draft

E : Writing - Review & Editing

Vi : Visualization

Su : Supervision

P : Project administration

Fu : Funding acquisition

### CONFLICT OF INTEREST STATEMENT

The authors declare no conflict of interest.

### ETHICAL APPROVAL

This research did not involve any experimentation on human participants or animals.

### DATA AVAILABILITY

Data availability does not apply to this paper.




### REFERENCES

- [1] S. Lamultree, M. Phalla, P. Kunkritthanachai, and C. Phongcharoenpanich, "Design of a circular patch antenna with parasitic elements for 5G applications," *IJE Transactions C: Aspects*, vol. 36, no. 9, pp. 1686-94, Sep. 2023, doi: 10.5829/ije.2023.36.09c.13 23.
- [2] Y. Frist, M. Elhabchi, and M. N. Srfi, "A compact multiband antenna based on metamaterial for L-band, WiMax, C-band, X-band, and Ku-band applications," *TELKOMNIKA*, vol. 22, no. 1, pp. 1-15, Feb. 2024, doi: 10.12928/telkomnika.v22i1.25204
- [3] M. Marzouk, Y. Rhazi, I. H. Nejadi, and M. Saih, "A new printed multiband fractal triangular antenna for wireless application," *TELKOMNIKA*, vol. 22, no. 1, pp. 55-64, Feb. 2024, doi: 10.12928/telkomnika.v22i1
- [4] Y. Amraoui *et al.*, "High gain MIMO antenna with multiband characterization for terahertz applications," *Sci.Afr.*, vol. 26, Dec. 2024, doi: 10.1016/j.sciaf.2024.e02380
- [5] Y. Amraoui *et al.*, "Terahertz dual-band antenna design with improved performances using FSS-based metasurface concept for wireless applications," *Sci.Afr.*, vol. 27, Mar. 2025, doi: 10.1016/j.sciaf.2025.e02566
- [6] K. Sreelakshmi, G. S. Rao, and M. N. V. S. S. Kumar, "A compact grounded asymmetric coplanar strip-fed flexible multiband reconfigurable antenna for wireless applications," *IEEE Access*, vol. 8, pp. 194497-194507, Oct. 2020, doi:10.1109/ACCESS.2020.3033502
- [7] C. Camacho-Gomez *et al.*, "Design of a multi-band microstrip textile patch antenna for LTE and 5G services with the CRO-SL ensemble," *Appl. Sci.*, vol. 10, no. 3, p. 1168, Feb. 2020, doi:10.3390/app10031168




- [8] A. Surendran *et al.*, “A dual-band modified franklin mm-wave antenna for 5G wireless applications,” *Appl. Sci.*, vol. 11, no. 2, p. 693, Jan. 2021, doi:10.3390/app11020693
- [9] K. Ramahatla, M. Mosalaosi, A. Yahya, and B. Basutli, “Multiband reconfigurable antennas for 5G wireless and CubeSat applications: A review,” *IEEE Access*, vol. 10, no. 9, pp. 40910–40931, Jan. 2022, doi: 10.1109/ACCESS.2022.3166223
- [10] L. X. Xiaochi, Y. Chen, S. Guo, and S. Yang, “An electromagnetic-transparent cascade comb dipole antenna for multi-band shared-aperture base station antenna array,” *IEEE Trans. Antennas Propag.*, vol. 70, no. 4, pp. 2750–2759, Apr. 2022, doi: 10.1109/TAP.2021.3137511
- [11] R. K. Mistri *et al.*, “Quad element MIMO antenna for C, X, Ku, and Ka-band applications,” *Sensors*, vol. 23, no. 20, Oct. 2023, doi:10.3390/s23208563
- [12] R. G. L. de Mello, A. C. Lepage, and X. Begaud, “A low-profile, triple-band, and wideband antenna using dual-band AMC,” *Sensors*, vol. 23, no. 4., p. 1920, Feb. 2023, doi:10.3390/s23041920
- [13] R. Yazdani, H. Aliakbarian, A. Sahraei, and G. A. E. Vandenbosch, “A compact triple-band dipole array antenna for selected sub 1 GHz, 5G and WiFi access point applications,” *IET Microwaves, Antennas & Propagation*, vol. 15, no. 15, pp.1866–1876, Oct. 2021, doi: 10.1049/mia2.12200
- [14] D. Sharma *et al.*, “A compact wearable textile antenna for NB-IoT and ISM band patient tracking applications,” *Sensors*, vol. 24, no. 15, p. 5077, Aug. 2024, doi: 10.3390/s24155077
- [15] K. V. Babu *et al.*, “A compact planar MIMO inverted-F antenna (PIFA) for sub-6 GHz 5G communication and IoT wireless networks applications,” *Int. J. Commun. Syst.*, Nov. 2024, doi: 10.1002/dac.6026
- [16] Y. Sun *et al.*, “Tri-band dual-polarized shared-aperture antenna arrays with wide-angle scanning and low profile for 5G base stations,” *IEEE Trans. Antennas Propag.*, vol.72, no.3, pp.2455–2467, Jan. 2024, doi: 10.1109/TAP.2024.3358611
- [17] C. K. Lin, D. B. Lin, H. C. Lin, and C. C. Lin, “Design of a compact multiband monopole antenna with MIMO mutual coupling reduction,” *Sensors*, vol. 24, no. 7, p. 5495, Aug. 2024, doi: 10.3390/s24175495
- [18] S. Lamultree, W. Thanamalapong, S. Dentri, and C. Phongcharoenpanich, “Tri-band bidirectional antenna for 2.4/5 GHz WLAN and Ku-band applications,” *Appl. Sci.*, vol. 12, no. 12, p.5817, Jun. 2022, doi: 10.3390/app12125817
- [19] J. Hou *et al.*, “MIMO 5G smartphone antenna with tri-band and decoupled elements,” *Sensors*, vol. 23, no.11, p. 5186, May 2023, doi: 10.3390/s23115186
- [20] R. Kumar, G. S. Saini, and D. Singh, “Compact tri-band patch antenna for Ku band applications,” *PIERC*, vol. 103, pp. 45-58, 2020, doi:10.2528/PIERC20013101
- [21] S. Y. A. Fatah *et al.*, “Design and implementation of UWB slot-loaded printed antenna for microwave and millimeter wave applications,” *IEEE Access*, vol. 9, pp. 29555 – 29564, Feb. 2021, doi: 10.1109/ACCESS.2021.3057941
- [22] B. Chinnagurusamy, M. Perumalsamy, and T. S. A. Samuel, “Design and fabrication of compact triangular multiband microstrip patch antenna for C- and X-band applications,” *Int. J. Commun. Syst.*, vol. 34, no. 3, Aug. 2021, doi: 10.1002/dac.4939
- [23] J. Li, J. Huang, H. He, and Y. Wang, “An ultra-thin multi-band logo antenna for internet of vehicles applications,” *Electronics*, vol. 13, no. 14, p. 2792, 2024, doi: 10.3390/electronics13142792
- [24] Y. Rahayu, D. R. A. Pangestu, and C. H. Ku, “Compact triple-band monopole antenna with ACS-fed for IoT devices on WLAN/WiMAX/5G/V2X networks,” *IJEETC*, vol. 14, no. 1, pp. 43-50, 2025, doi:10.18178/ijeetc.14.1.43-50
- [25] H. Y. Li, J. X. Du, X. Yan, and S. Gao, “Low-profile all-textile multiband microstrip circular patch antenna for WBAN applications,” *IEEE Trans. Antennas Propag.*, vol. 21, no. 4, pp. 779–783, 2022, doi: 10.1109/LAWP.2022.3146435
- [26] V. Nanthagopal, and J. Paramasivam, “Coaxial pin-fed multiband fractal square antenna for satellite applications,” *PIERC*, vol. 138, pp. 247-259, 2023, doi:10.2528/PIERC23062201
- [27] R. Wang, B. Wang, and X. Ding, “Planar array with bidirectional elements for tunnel environments,” *Sci. Rep.*, vol. 7, no. 1, p. 15421, 2017, doi: 10.1038/s41598-017-15817-4
- [28] G. Dong, X. Li, and A. Zhang, “Spoof surface plasmon polariton endfire antenna possessing bidirectional and unidirectional radiation pattern,” *IEEE Trans. Antennas Propag.*, vol. 21, no. 1, pp. 69 – 73, 2022, doi:10.1109/LAWP.2021.3118442
- [29] N. Liu *et al.*, “Radiation pattern reshaping of a narrow slot antenna for bandwidth enhancement and stable pattern using characteristic modes analysis,” *IEEE Trans. Antennas Propag.*, vol. 70, no. 1, pp. 726–731, 2022, doi: 10.1109/TAP.2021.3098535
- [30] F. Ge, H. Zhao, S. Li, and X. Yin, “Bidirectional scanning antenna based on surface wave mode,” *IEEE Trans. Antennas Propag.*, vol. 21, no. 8, pp. 1592–1596, 2022, doi: 10.1109/LAWP.2022.3174879
- [31] L. Smith, and S. Lim, “Design of a compact, planar, wideband, overlapped, bow-tie antenna in a single layer with stable bi-directional radiation patterns,” *Appl. Sci.*, vol. 214, no. 20, p. 9555, Oct. 2024, doi:10.3390/app14209555.
- [32] Computer Simulation Technology, “Microwave Studio,” *Academic Version*, 2023. <https://sigmasolutions.co.th/en/cst-studio-suite>
- [33] C. A. Balanis, *Antenna Theory: Analysis and Design*. 4<sup>th</sup> ed, Wiley, 2016. ISBN: 9781118642061
- [34] R. E. Collin, *Foundations for Microwave Engineering*, McGraw-Hill, New York, 1992. ISBN 0780360311

## BIOGRAPHIES OF AUTHORS






**Suthasinee Lamultree**    received the B. Eng., and M. Eng., in Telecommunication Engineering from King Mongkut’s Institute of Technology Ladkrabang, Thailand, in 2000 and 2003, respectively. In 2009, she received her D.Eng., in Electrical Engineering from the same institute. In 2016, she joined the Department of Electronics and Telecommunication Engineering, Faculty of Engineering, Rajamangala University of Technology Isan Khonkaen Campus, Khonkaen, Thailand. Her research interests include antenna design, microwave technology, and wireless communication systems. She can be contacted at email: suthasinee.la@rmuti.ac.th.






**Wutthipong Thanamalapong**    received the B.Eng., in Electrical Engineering from the Faculty of Engineering, Khonkaen University in 2012 and the M.Eng. in Electrical Engineering from the Faculty of Engineering, Rajamangala University of Technology Isan Khonkaen Campus, Thailand, in 2022. His research interests include antenna design and electrical systems. He can be contacted at email: wutthipong.th@rmuti.ac.th, noom.wu.th@gmail.com.



**Kanawat Nuangwongsa**    received his B.Eng., M.Eng., and D.Eng., degrees from King Mongkut's Institute of Technology Ladkrabang (KMITL), Bangkok, Thailand, in 2007, 2009, and 2016, respectively. Currently, he joined the Department of Electronics and Telecommunication Engineering, Faculty of Engineering, Rajamangala University of Technology Isan (RMUTI) Khonkaen Campus, Khonkaen, Thailand. His research interests include antenna design, rf propagation modeling, microwave technology, and wireless communication systems. He can be contacted at email: kanawat.nu@rmuti.ac.th.



**Charinsak Saetiaw**    received his Ph.D., in Telecommunication Engineering from Suranaree University of Technology in 2016. He is an Assistant Professor in the Department of Electronics and Telecommunication Engineering, Faculty of Engineering, at Rajamangala University of Technology Isan, Khon Kaen Campus. His research focuses on antenna design, wireless communication, telecommunication engineering, emerging technologies, and innovative applications. His work interests are the development of antennas for 4G and 5G applications, 3D printing and conductive materials, and advancing applications in wearable and vehicular communication systems. He can be contacted at email: charinsak.sa@rmuti.ac.th.